Earth and Planetary Science Letters 294 (2010) 1–7

Contents lists available at ScienceDirect

Earth and Planetary Science Letters

journal homepage: www.elsevier.com/locate/epsl

Kamacite blocking temperatures and applications to lunar magnetism

Ian Garrick-Bethell [a,*], Benjamin P. Weiss [b]

[a] Department of Geological Sciences, Brown University, Box 1846, Providence, RI 02912, United States
[b] Department of Earth, Atmospheric and Planetary Sciences, Massachusetts Institute of Technology, 77 Massachusetts Avenue, Cambridge, MA 02139, United States

ARTICLE INFO

Article history:
Received 18 September 2009
Received in revised form 7 February 2010
Accepted 9 February 2010
Available online 2 April 2010

Editor: T. Spohn

Keywords:
kamacite
lunar
moon
blocking temperature
magnetism
iron
paleomagnetism

ABSTRACT

The long-term stability of remanent magnetization is a requirement for paleomagnetic studies. Here we present calculations that predict the magnetic relaxation times of single domain crystals of the iron–nickel mineral kamacite as a function of their time–temperature history. Kamacite is one of the most abundant ferromagnetic minerals in the solar system and is the dominant remanence carrier on the Moon. We perform these calculations for a variety of grain sizes, times, and temperatures to derive a broad view of the remanence stability of kamacite over geologic timescales. Previously, such blocking temperature calculations were only available for the common Earth minerals magnetite, hematite, and pyrrhotite. Our results show that remanence in kamacite-bearing lunar samples is stable against typical thermal perturbations during the last several billion years of lunar history and residence on Earth. Our findings indicate that lunar paleomagnetism cannot be entirely an artifact due to sample storage in the Earth's magnetic field. Future paleomagnetic studies of iron-bearing samples can use our blocking temperature diagram to determine the effects of geologic heating events on magnetic remanence.

1. Introduction

On Earth, time–temperature events such as thermal metamorphism are often important sources of a rock's natural remanent magnetization (NRM). Long-term heating in a magnetic field may impart a viscous overprint on the NRM and obscure the primary record of magnetization. Pullaiah et al. (1975) computed simple diagrams to quantify this effect for the common Earth minerals magnetite and hematite. Nearly three decades later, similar calculations and diagrams were published for pyrrhotite (Dunlop et al., 2000; Weiss et al., 2000). These diagrams are based on theory developed by Néel (1949) and illustrate the tendency of an assemblage of single domain grains to relax its magnetization as a result of different time–temperature histories.

On the Moon and in some meteorites, the primary carrier of remanent magnetization is native iron, which is usually alloyed with a minor amount of nickel and cobalt to form the body-centered cubic mineral kamacite. Although nearly ubiquitous on the lunar surface, kamacite is virtually absent from the Earth's crust. Because of the complexities and unfamiliarity of working with kamacite, some scientists have rightfully questioned the reliability of lunar rock magnetism studies. One problem is that the NRM in kamacite may be a mixture of thermoremanent magnetization (TRM) and phase-transformation crystallization remanent magnetization (CRM) due to recrystallization during cooling (Wasilewski, 1974) (Section 2). Another problem is the common prevalence of multidomain grains, which do not have discrete blocking and unblocking temperatures. A third problem is that chemical alteration of kamacite during heating often confounds thermal paleointensity experiments. A final problem, which forms the subject of this paper, is the uncertain effect of long time–temperature histories on the stability of the remanent magnetization. For example, most lunar samples have been exposed to diurnal surface temperature changes between 0–100 °C for hundreds of millions of years, leaving open the possibility that their NRM has decayed in the presumably low-field environment of the recent Moon (Dunlop and Özdemir, 1997). Apollo samples have also been stored at room temperature in the Earth's field for several decades, which has imparted a viscous remanence. In this paper, we follow the methodology of Pullaiah et al. (1975) to derive time–temperature stability diagrams for kamacite remanence. While these diagrams do not perfectly predict unblocking temperatures and do not apply to multidomain grains, they can provide guidance for samples with mixtures of single and multidomain crystals. They have particular relevance for paleomagnetic studies of lunar breccias and soils, which contain significant amounts of superparamagnetic and single domain grains.

2. Iron–nickel alloys

Since the chemistry and magnetism of iron–nickel compounds is quite complex and not often discussed in the context of lunar and

* Corresponding author. Tel.: +1 401 301 5237.
E-mail address: Ian_Garrick-Bethell@brown.edu (I. Garrick-Bethell).

0012-821X/$ – see front matter © 2010 Published by Elsevier B.V.
doi:10.1016/j.epsl.2010.02.013

meteorite magnetism, we first review these issues. This discussion is important for establishing the range of nickel content for which our kamacite calculations are relevant.

2.1. Equilibrium phase diagram

Upon slow cooling from the liquid state, pure iron at low pressure (< ~5 GPa) passes through a series of equilibrium solid-state phases known as delta (δ), gamma (γ), and alpha (α), in order of their appearance (Swartzendruber et al., 1993; Anderson and Isaak, 2000; Cacciamani et al., 2006). These phase changes correspond to crystallographic transformations from body centered cubic (bcc) to face centered cubic (fcc), and finally back to bcc, respectively. In steel formation, where iron is mixed with carbon, the three crystalline phases are known as δ, austenite, and ferrite, respectively. When iron is alloyed with nickel (as typically found in meteorites and lunar rocks), these phases are referred to as δ, taenite, and kamacite, respectively, as shown in the simplified equilibrium Fe–Ni phase diagram in Fig. 1 (at atmospheric pressure) (Cacciamani et al., 2006). Since carbon and nickel prefer fcc solvents, both constituents will diffuse out of ferrite (kamacite) into austenite (taenite) during cooling in the $\alpha+\gamma$ two-phase stability field. This exsolution process leads to mixtures of taenite enriched in nickel, and kamacite depleted in nickel, relative to the bulk Ni content. Below about 345 °C, the $\alpha+\gamma$ stability field is believed to become a field with α + ordered $FeNi_3$ (γ', also known as awaruite) (Cacciamani et al., 2006). Below ~400 °C and for low bulk nickel compositions, the kinetics of the formation of awaruite can be very slow (Romig and Goldstein, 1980), but it has been observed in meteorites (Yang et al., 1997) with <10% Ni.

Kamacite and high nickel taenite (>~30% Ni (Dunlop and Özdemir, 1997; Goldstein et al., 2009)) are both ferromagnetic. For bulk alloy compositions with <3% Ni, equilibrium cooling produces a pure thermoremanent magnetization (TRM) in the kamacite phase, which wholly makes up the cooled metal before and after the Curie temperature is reached. Kamacite with 3% Ni has a Curie temperature of approximately 760 °C (Fig. 1). For bulk compositions with >3% Ni, kamacite and taenite continually equilibrate below the Curie temperature during cooling to produce a phase-transformation CRM in the kamacite (as well as in taenite if it is high enough in Ni to be ferromagnetic). It is not known if such a remanence mechanism retains a memory of TRM acquired at earlier equilibrium states (Dunlop and Özdemir, 1997). However, phase diagrams often depict a Curie temperature line for compositions up to about 7% Ni where the Curie temperature line intercepts the γ phase. Curie temperature measurements of kamacite with >3 Ni% can be made by rapid cooling to form a supersaturated nonequilibrium α phase (see below) (Peschard, 1925). The alloy is then heated relatively quickly to measure the Curie temperature before chemical equilibration alters the TRM-carrying supersaturated material.

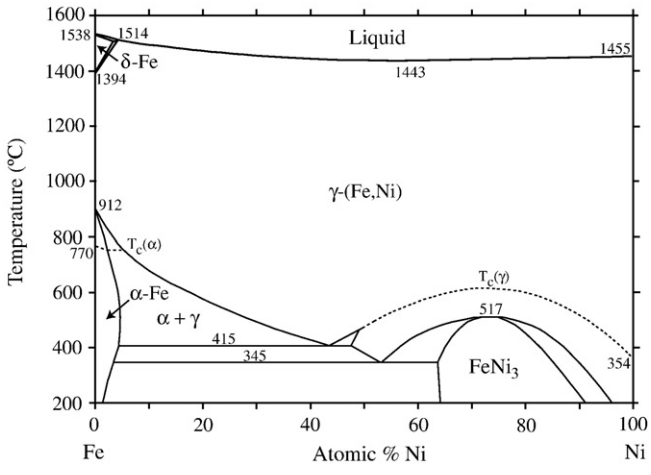

Fig. 1. Equilibrium phase diagram for the Fe–Ni system from (Cacciamani et al., 2006). The dashed lines show the Curie temperatures (T_c) for taenite and kamacite.

2.2. Non-equilibrium transformations

The equilibrium transformations described in the previous section depend heavily on cooling rate. Volume diffusion kinetics can be very slow in Fe–Ni alloys, so non-equilibrium taenite and kamacite compositions may be the end products of slow cooling. The diffusion rates for the decomposition of taenite into taenite plus kamacite can eventually slow to a point where equilibrium will not be reached over geologic timescales, even at modest temperatures. Therefore, intermediate non-equilibrium taenite–kamacite mixtures may freeze in. An example of this process includes the Widmanstätten structures in iron meteorites (Goldstein et al., 2009). Derived equilibrium phase diagrams may illustrate the thermodynamic preferences of an alloy, but the domination of kinetics often limits their practical use.

Depending on the cooling rate, a number of different mineral microstructures can develop in Fe–Ni alloys as a result of composition-invariant transformations. An example is the martensitic transformation, in which a supersaturated bcc structure forms by a shearing dislocation in the crystal lattice. According to Wilson (1994), there are six different composition-invariant transformations in the nickel–iron system; equi-axed ferrite, massive ferrite, Widmanstätten ferrite, bainitic ferrite, lath-martensite (classic martensite, also known as "massive martensite"), and twinned martensite. These transformations may also occur in pure iron, since they are crystal lattice dislocations that do not require the presence of solute atoms (Bhadeshia, 1985). However, the addition of a solute such as nickel can lower the start temperature of these reactions by several hundred degrees. Cooling rates to achieve these transformations can also vary by six orders of magnitude depending on the reaction types and solute content. Many studies have been performed on the cooling rates necessary to achieve a given microstructure, e.g. (Massalski, 1984; Chong et al., 1998; Wilson and Chong, 2002). In addition, the formation of awaruite from taenite below ~345 °C is suppressed by formation of metastable ordered states (Fe_3Ni and FeNi, tetrataenite), but these states are not likely to appear for <5–15% Ni, assuming cooling times substantially faster than meteorites (~1–100 °C/M.y.) (Reuter et al., 1989; Swartzendruber et al., 1993; Reisener and Goldstein, 2003).

Some aspects of the effect of cooling rate, microstructure, and nickel content on kamacite magnetic properties have been examined by Wasilewski (1974, 1981). Wasilewski (1974) proposed nine new remanence mechanisms for Fe–Ni alloys based on microstructure, and included samples transformed by both the massive and martensite transformations. Further experiments (Wasilewski, 1981) concluded that microstructure is a major factor in determining intensity of remanence and stability to AF demagnetization. Other solutes such as carbon, cobalt, and phosphorous can alter the likelihood and nature of phase transformations. Since almost all lunar kamacite has some nickel, cobalt, or other contaminants, and its grain size is often multidomain, its remanence characteristics may be complex and include CRM. However, even for bulk alloys with >3% Ni for which some CRM is predicted (Section 2.1.), we note that equilibrium reactions may not go to completion. Instead, they may form nonequilibrium supersaturated kamacite at sub-Curie temperatures high enough to block in significant TRM, and lesser minor amounts of CRM. For example, Wilson and Chong (2002) found supersaturated Widmanstätten ferrite and equi-axed ferrite after cooling a 9% Ni alloy at various rates. Néel theory is directly applicable to the TRM of such supersaturated materials, but caution must be used for grains with high blocking temperatures that may be dominated by CRM. This same caution should be used when considering paleomagnetic heating experiments.

Clearly, the remanence of metals is more complicated than that of magnetite. Efforts must be made to understand the thermal history of the sample in question before applying our calculations, which are strictly for TRM in single domain crystals. With these complexities in mind, we will calculate the relaxation times for homogeneous single domain bcc iron crystals and assess their validity for low nickel and cobalt alloys.

3. Time–temperature relaxation calculation

3.1. Single domain iron

Our calculations follow those of Pullaiah et al. (1975). The relaxation time, τ, of a single domain particle in zero field can be written (Néel, 1949):

$$\frac{1}{\tau} = C\, exp\left(\frac{-\mu_o v J_s(T) H_c(T)}{2kT}\right), \tag{1}$$

where C is the characteristic frequency of thermal oscillation, μ_o is the magnetic constant, v is the particle volume, $J_s(T)$ is the temperature dependent spontaneous magnetization, $H_c(T)$ is the temperature dependent microscopic coercivity, k is Boltzmann's constant, and T is temperature in kelvins. Grains with a given v, H_c, and J_s will unblock their magnetization after heating to a temperature T for an unblocking time τ. We use a parameterization of the $J_s(T)$ curve from (Kuz'min, 2005):

$$J_s(T/T_c) = J_o\left(1 - s(T/T_c)^{3/2} - (1-s)(T/T_c)^p\right)^{1/3} \tag{2}$$

where J_o is the saturation magnetization at $T = 0$ K, equal to 1750 kA/m, T_c is the Curie temperature, 1044 K, and $s = 0.35$ and $p = 4$ are empirically determined parameters (Fig. 2). Eq. (1) is based on experimental data from (Crangle and Goodman, 1971). Crangle and Goodman (1971) measured 99.95% pure iron and make no remarks about rapid cooling in their work, so it is unlikely their data are greatly affected by nonequilibrium microstructure effects. Other experimental and theoretically determined curves for $J_s(T)$ (Bozorth, 1951) produce similar blocking temperature results as those presented here.

Complete data for the temperature dependence of the microscopic coercivity of iron do not appear in the literature. Fortunately, we may make a reasonable approximation for $H_c(T)$ by examining its dependence on the magnetic anisotropy of the grain and $J_s(T)$. Single domain magnetic anisotropy is due to three different effects: grain shape (shape anisotropy), grain crystal structure (magnetocrystalline anisotropy), and stress on the grain (magnetoelastic anisotropy). The $H_c(T)$ dependence on these three anisotropies is, respectively:

$$H_{c,s}(T) = NJ_s(T) \tag{3a}$$

$$H_{c,c}(T) = \frac{4}{3}\frac{|K_1(T)|}{\mu_o J_s(T)} \tag{3b}$$

$$H_{c,r}(T) = \frac{3|\lambda\sigma|}{\mu_o J_s(T)}, \tag{3c}$$

where N is the difference between the demagnetizing factors in the easy and hard directions, $K_1(T)$ is the first term of the magnetocrystalline anisotropy constant, and λ is the polycrystalline magnetostriction constant at saturation. At 20 °C $K_1 = 4.8\times10^4$ J/m^3 and $\lambda = -7\times10^{-6}$ (Dunlop and Özdemir, 1997).

We wish to understand which of these three anisotropies contributes the most to $H_c(T)$. We first note that at 20 °C, $H_{c,s}$ is larger than $H_{c,c}$ when $N \geq 0.017$, which occurs when grains are elongated by 4.4% or more, using the prolate ellipsoid shape demagnetizing factors from Eqs. 2.20 and 2.21 of (Cullity, 1972). To determine if this relationship holds true for all temperatures, we use the temperature dependent $K_1(T)$ function presented by Bozorth (1951) (Fig. 12–11, scanned and digitized) and shown in Fig. 3. Values of $H_{c,s}$ and $H_{c,c}$ are plotted in Fig. 4 with a value of $N = 0.017$ for $H_{c,s}$, demonstrating that $H_{c,s}$ continues to dominate $H_{c,c}$ at temperatures >20 °C. For magnetoelastic anisotropy, even if we use the ultimate tensile strength of iron, $\sigma \approx 400$ MPa, $H_{c,c}$ is 7 times larger than $H_{c,r}$ at 20 °C (Fig. 4). Therefore, we conclude that for nearly all grain shapes and stress states, shape anisotropy dominates the coercivity of kamacite: $H_c = NJ_s(T)$. Pullaiah et al. reach the same conclusion for magnetite grains elongated by ≥10%.

Taking $C = 10^{10}$ Hz (Pullaiah et al., 1975) we compute Eq. (1) for a variety of temperatures (Fig. 5). For example, we can see that grains with a 1000 s (typical laboratory heating time) blocking temperature of 375 °C will also unblock after heating at 125 °C in zero field for 3 My. Relaxation in a non-zero field changes (1) to:

$$\frac{1}{\tau} = C\, exp\left(\frac{-\mu_o v J_s(T) H_c(T)}{2kT}\left(1 - \frac{|H_o|}{H_c}\right)^2\right) \tag{4}$$

where H_o is the ambient field (Eq. 8.17 of (Dunlop and Özdemir, 1997)). For $H_o = 0.1$ mT compared to $H_c(T) = 37$ mT (assuming shape

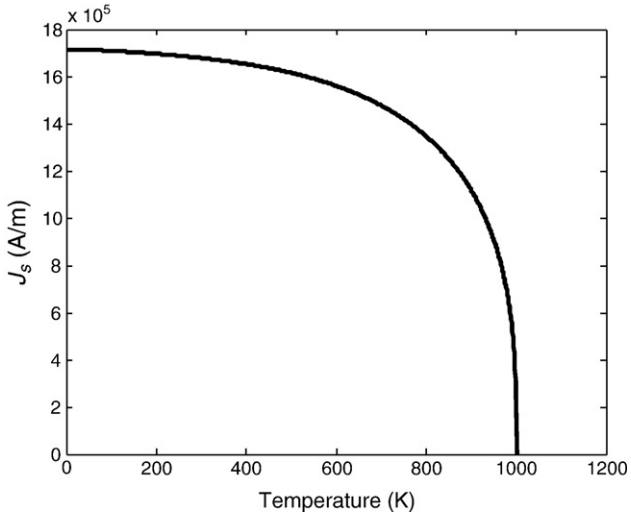

Fig. 2. Saturation magnetization $J_s(T)$ vs. temperature for pure iron, from the parameterization of (Kuz'min, 2005).

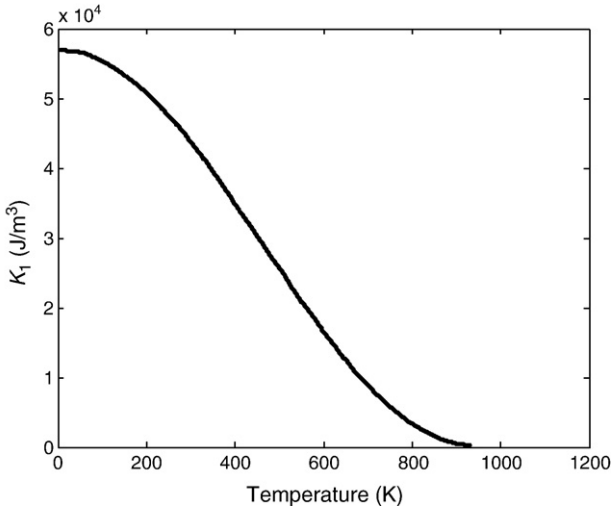

Fig. 3. First order term of the magnetocrystalline anisotropy constant (K_1) vs. temperature for pure iron (Bozorth, 1951).

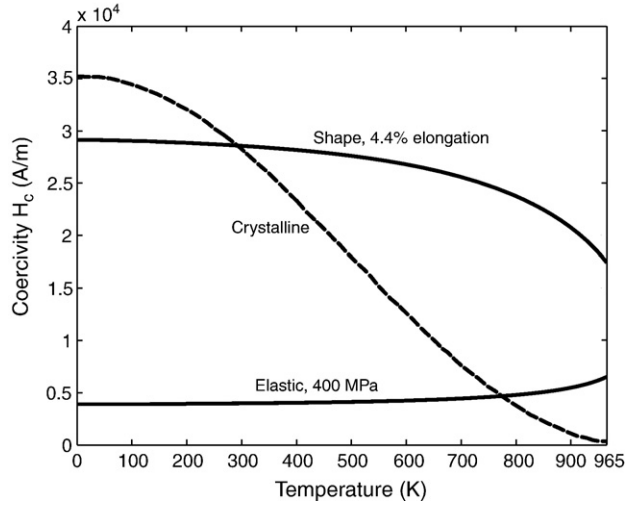

Fig. 4. Coercivity from shape anisotropy ($H_{c,\,s}$), magnetocrystalline anisotropy ($H_{c,\,c}$), and magnetoelastic anisotropy ($H_{c,\,r}$) for kamacite as a function of temperature.

anisotropy, $J_s(20°C) = 1715$ kA/m (Dunlop and Özdemir, 1997), and $N = 0.017$), we obtain $(1 - H_o/H_c)^2 = 0.995$. Therefore predictions for τ from Eq. (4) for typical geomagnetic fields are essentially identical to that from Eq. (1).

3.2. Extrapolation to low nickel and cobalt alloys

Although we have calculated blocking temperature relations for pure iron, we can apply these calculations to low nickel alloys because they have similar $J_s(T)$, $H_c(T)$, and T_c. Most lunar kamacite has Ni<10% (Nagata et al., 1974), and Co<3% (Ryder et al., 1980). The Curie temperature of α iron decreases slowly up to about 15% nickel ($T_c = 700$ °C) (Swartzendruber et al., 1993). Measurements show that the saturation induction at 20 °C, which can be used as a proxy for J_s(20 °C), increases by only 3% with the addition of 5% Ni, and then decreases again to the zero nickel value at 10% Ni, and 3% below the zero Ni value at 15% Ni (Bozorth, 1951) (see his Fig. 5–8). In addition, measurements of the saturation induction as a function of temperature at 40% Ni follow a function that is similar in shape to that at 0% Ni (Bozorth, 1951) (see his Fig. 5–10). The value of K_1 decreases monotonically to ~40% of its 0% Ni value at 16% Ni, at room temperature (Tarasov, 1939), which implies that shape anisotropy continues to dominate at this Ni concentration. Data on the change in K_1 with temperature could not be found for higher nickel contents, but the slowly and monotonically changing values of K_1 with temperature for pure Ni and Fe ((Bozorth, 1951) Fig. 12–11 and 12–13) make it likely that shape anisotropy continues to dominate the anisotropy contribution to H_c at higher temperature.

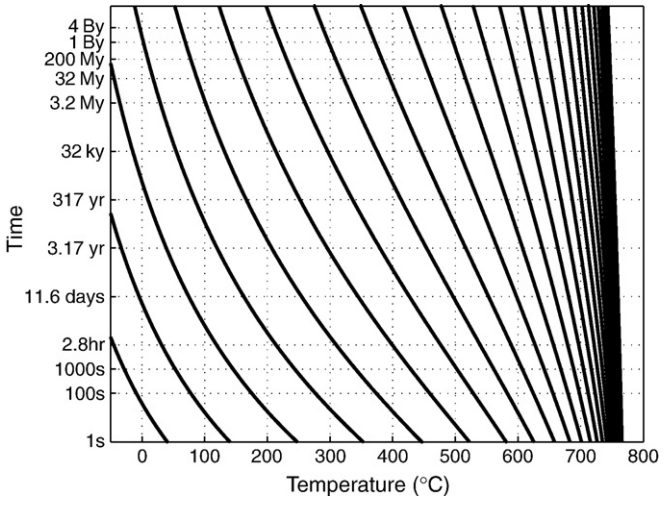

Fig. 5. Time–temperature unblocking relationships for single domain kamacite grains (100% Fe). Each curve shows the time required to demagnetize or remagnetize a grain (in weak fields) for a particular value of the product $vH_c(T)$, where v is the grain volume and $H_c(T)$ is its microscopic coercivity. The curves here were calculated for prolate ellipsoidal grains with axial ratios (length/width) of 1.10 (dominated by shape anisotropy) and widths from 14 to 50 nm, although they can represent the demagnetization behavior for grains with any value of vH_c. The critical superparamagnetic threshold (diameter at which a grain will demagnetize after 100 s at room temperature) is ~14 nm, in good agreement with other estimates (Dunlop and Özdemir, 1997).

In summary, the slowly varying T_c and J_s(20 °C) up to at least 15% Ni, the similar shape of the $J_s(T)$ function at high nickel, and the smooth behavior of the anisotropy functions suggest that the above equations and assumptions for 0% Ni will be fairly accurate for up to about 15% Ni (which would be nonequilibrium supersaturated kamacite). For instance, if one were to use the reduced Curie temperature for 15% Ni (700 °C), a J_s(0 °C) value equal to the 0% Ni value (the value at 15% Ni is ~97% of its 0% Ni value, based on (Bozorth, 1951) Fig. 5–8), and the same $J_s(T)$ function shape, the estimated change in the time-temperature curves can be determined. Under these assumptions, 15% Ni curves initially overlapping the 0% Ni curves at long blocking times (~4 B.y.) diverge and unblock at slightly lower temperatures at unblocking times of 1000 s. The divergence increases at higher temperatures. For example, for curves initially overlapping at 4 B.y., at 100 °C the unblocking temperatures for 1000 s are nearly identical, while at 500 °C the unblocking temperatures are reduced by 30 °C to 470 °C, and at 700 °C the unblocking temperatures are reduced by 50 °C to 650 °C. These uncertainties (particularly relating to the Ni-dependence of the Curie temperature) may be too large for some applications, and we end by noting that our calculations are therefore strictly only accurate for 0% Ni iron.

For iron with < 20% Co, T_c rises slowly with Co content, increasing by a few degrees at 3% Co (Nishizawa and Ishida, 1993). $J_s(T)$ data could not be found for low Co alloys, but the saturation induction at 20 °C decreases less than 5% for Co <10% (Bozorth, 1951) (see his Fig. 5–80). We could not find data on the temperature dependence of K_1 for Co <10%, but for pure cobalt K_1 changes slowly and monotonically as a function of temperature (Bozorth, 1951) (see his Fig. 12–12). Given the small and monotonic changes in T_c, K_1, and saturation induction for alloys up to 10% Co, we conservatively apply our calculations to kamacite with <3% Co. Using the available data for 3% Co would not significantly change our blocking temperature calculations.

For bulk nickel content greater than about 3%, Curie temperatures become less well defined for two reasons. The first is that if the metal is assumed to have been in complete equilibrium during cooling and subsequent heating, the magnetic remanence will be altered by crystal structure changes in the kamacite + taenite stability field (Section 2 and Fig. 1). The second is that the metal may contain nonequilibrium reaction products that include kamacite with varying amounts of nickel; the Curie temperatures of these intergrown phases are often not known. These complications are probably more significant for meteorites, where large multidomain grains of iron with high nickel contents may have formed with very slow cooling times. In any case, the blocking temperature calculations are not affected by these complications, as long as the user is aware of the microstructure of the kamacite in the sample.

4. Predictions

4.1. Lunar thermal histories

We can use Fig. 5 to predict the long-term stability of lunar rock magnetism for three idealized thermal processes that nearly all Apollo samples have likely experienced: (Case 1) burial in the near-surface

regolith, (Case 2) exposure to solar heating on the lunar surface, and (Case 3) residence on Earth. While these predictions are for lunar samples, similar thermal histories could be applied to kamacite-bearing meteorites.

The temperature gradient of the lunar regolith is about −1.7 °C/m (Heiken et al., 1991), and most regolith is on the order of 10 m thick (Wilcox et al., 2005). Below the regolith, thermal gradients decrease markedly, so that rocks are not heated to high temperatures (>100 °C) in the upper few kilometers from which most lunar samples have originated. At the surface, the diurnal temperature variation is −140 to +110 °C at the equator, but it is completely attenuated to a constant −20 °C at approximately 30 cm depth. Therefore, the minimum temperature lunar rocks could have experienced during their pre-surface history lasting for 1–4 B.y. is about −20 °C at ~30 cm. We conservatively assume −20 °C for our first part of the rocks' thermal history lasting for 1–4 B.y.

On the Moon, rocks are often brought to the upper few meters of the lunar surface before being fully exposed. Near-surface exposure ages calculated from spallation-produced elements range from 1–300 M.y. (Arvidson et al., 1975), but the depth of burial is not often resolved to 30 cm accuracy, leaving open the possibility that they experienced some diurnal heating. Particle tracks and microcraters have been used to calculate the "suntan" ages of rocks, which can often span 1–300 M.y. Therefore, the second part of the rock's history will be exposure to the diurnal surface wave at 100 °C lasting for 1–300 M.y. (assuming the rocks are only heated during half of each lunar day during this period gives nearly the same results).

For the third part of the rock's history we assume storage on Earth for ~10 yr at 20 °C.

We use Fig. 5 to calculate the 1000 s unblocking temperatures that will demagnetize the same grains affected by each of the above three idealized thermal histories. We assume there were negligible ambient magnetic fields on the Moon for the past 4 B.y. For Case 1, near-surface residence at −20 °C for 1–4 B.y. yields an unblocking temperature of about 215 °C. In Case 2, storage on the surface at 100 °C for 1–300 M.y. leads to an unblocking temperature of 325–375 °C. In Case 3, storage on Earth for 10 yr yields an unblocking temperature of 125 °C. Therefore, grains with unblocking temperatures up to 125 °C acquire magnetization from the Earth's field. This viscous contamination can be mostly removed by ~1 month of storage at 20 °C in zero field, which resets grains up to blocking temperatures of 85 °C. Additional histories such as mare volcanism heating, ejecta blanket heating, and shock heating, may also be explored using Fig. 5.

4.2. Thellier–Thellier paleointensity determination and ideal Arai plot

Thermal demagnetization experiments are useful in determining which grains carry remanence and how the remanence of those grains has been affected by viscous overprinting. The most robust thermal demagnetization technique for determining the paleofield H_o is the modified Thellier–Thellier double heating method (Thellier and Thellier, 1959). Briefly, rocks are heated to a given temperature, and their remaining remanent magnetization is measured after cooling in a zero field environment. The samples are then reheated to the same temperature and allowed to cool in an ambient field, H_a. Ideally, the NRM lost in the first step will be equal to the partial thermal remanent magnetization (pTRM) gained in the second step, up to a factor equal to the ratio H_o/H_a. Each double heating step is plotted as NRM remaining vs. pTRM gained (the Arai plot), for which a straight line indicates ideal single domain behavior with no thermal alteration, and the slope provides H_o/H_a.

Thellier–Thellier experiments are ideally suited for assessing our predictions because the incremental heating method allows the user to determine the effects of past thermal events without knowledge of the blocking temperature distribution in the rock. For example, it may be that a rock has few grain sizes with low blocking temperatures, such that most of its remanence is carried by higher blocking-temperature grains. Merely heating such a rock and measuring the decrease in NRM would reveal small changes in NRM at low temperatures and greater changes at higher temperatures. However, this would not unambiguously distinguish between there being few grains of low blocking-temperature, or a significant amount of low blocking-temperature grains that had relaxed in a low field environment. In a Thellier–Thellier experiment, if there are few grains within a given blocking temperature range, this will be reflected as small differences in the distances between heating steps at those blocking temperatures (in an Arai plot), but the slope of the line will nonetheless be indicative of the field that those grains have acquired.

The three previously outlined lunar thermal histories predict an idealized Arai plot with three different slopes (Fig. 6). The first slope at low temperature heating steps represents acquisition of viscous remanence in the Earth's field. The second slope is shallower, representing the loss of remanence over 2–4 B.y. in a presumably low field environment on the lunar surface. It represents both the time spent in the shallow subsurface at cold temperatures and at the surface at diurnal temperatures. The second slope should ideally begin near 125 °C and end at approximately 325–375 °C. The third slope is steeper than the second, indicating acquisition of an NRM in a lunar paleofield and should end at the Curie temperature, 771 °C. The third slope may or may not be higher than the first slope, or even zero, depending on the lunar paleofield strength. Fig. 8.14 of ref. (Dunlop and Özdemir, 1997) shows examples of similar effects in terrestrial basalts.

Unfortunately, comparison of our predictions with published data is presently difficult for four reasons: 1) With the exception of (Lawrence et al., 2008), previous Thellier–Thellier studies lack pTRM checks for alteration; 2) The most recent Thellier–Thellier experiments (Lawrence et al., 2008) were not performed in an atmosphere that controls oxidation (Sugiura et al., 1979); 3) Many previously studied samples may have had an overprinting IRM or shock remanent magnetization component that would have to be removed by alternating field demagnetization prior to heating (Gattacceca et al., 2007; Gattaccecaa et al., 2008; Lawrence et al., 2008; Garrick-Bethell et al., 2009); 4) Most lunar samples analyzed with Thellier–Thellier techniques are multidomain.

5. Discussion

Despite the above complications, our calculations should still be useful because there exist lunar samples with well-known metal

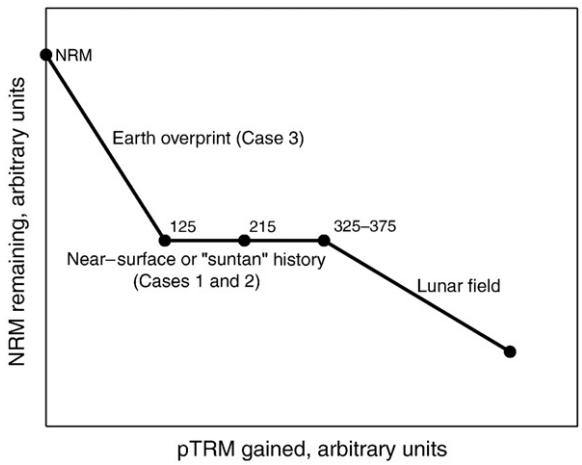

Fig. 6. Idealized Thellier–Thellier experiment for an Apollo rock containing a population of single domain kamacite grains (<15%Ni, <3% Co) with a spectrum of blocking temperatures between room temperature and the Curie point. Temperatures are indicated in degrees Celsius.

chemistry, cooling histories, and predominantly single domain grain sizes. Well-controlled Thellier–Thellier experiments on these samples may be possible. For example, Apollo samples 15498 and 60255 are glassy regolith breccias with relatively high ratios of saturation remanent magnetization (J_{rs}) to J_s of 0.09 and 0.06, respectively, and relatively high ratios of initial susceptibility per unit mass (χ_0) to J_s of 7×10^{-2} and 9×10^{-2} m/A, respectively, suggesting that they contain predominantly a mixture of single domain and superparamagnetic grains (Gose et al., 1973; Nagata et al., 1973; Pearce et al., 1973; Fuller and Cisowski, 1987). In fact, Gose and Carnes (1973) found that the time-dependent behavior of the magnetization of fine grained lunar breccias was well modeled by the same single domain Néel theory used in our analysis.

If a rock has multidomain grains it will thermally demagnetize at higher temperatures and have a concave up Arai plot. The source of this difficulty is that a multidomain grain acquires its magnetization by rearrangement and pinning of its domain walls (Dunlop and Özdemir, 1997). Increasingly elevated temperatures continually shift the domain magnetization through progressively lower-energy pinning states instead of rotating domains at a well-determined temperature as in single domain grains. This produces a spectrum of unblocking temperatures up to the Curie temperature (Dunlop and Özdemir, 1997). Therefore, on the lunar surface, it may be more difficult to demagnetize rocks with multidomain grains up to the blocking temperatures of 325–375 °C predicted by Fig. 6. This would suggest the predicted slope break near 325–375 °C would be an underestimate of the apparent unblocking temperature.

It is also important to note that there may be a magnetostatic interaction effect operating near 300 °C in lunar Thellier–Thellier studies, possibly further confounding predictions made from Fig. 5. Between 250–300 °C Pearce et al. (1976) and Chowdhary et al. (1987) observed discontinuities in Thellier–Thellier heating experiments and pTRM acquisition experiments in a variety of lunar rocks. They suggested that troilite (FeS), a phase commonly found in contact with kamacite, was interacting with the adjacent kamacite, either through a self-reversal or self-demagnetizing mechanism. These processes require that troilite, an antiferromagnet, behave ferromagnetically due to defect magnetizations. Because troilite has a Néel temperature of 320 °C, it may exert the greatest effect on the Arai plot below these temperatures.

Finally, it is worth discussing the effect of our predictions on room temperature techniques for measuring lunar paleofields. Some studies of lunar samples have crudely attempted to estimate the paleofield by normalizing NRM by saturation isothermal remanent magnetization (SIRM) (Sugiura and Strangway, 1980). The thermal demagnetizing effects of the lunar surface means that the NRM/SIRM technique of measuring the paleofield is only measuring grains with unblocking temperatures above 325–375 °C, assuming the sample does not have a contaminating IRM (Garrick-Bethell et al., 2009). Therefore, this technique may underestimate the paleofield by a factor of almost two, assuming the sample has evenly distributed blocking temperatures and has a significant remanence carried by single domain grains. We note that Dunlop et al. (1973) found that at least one lunar sample had almost half of its grain population with blocking temperatures below 300 °C.

6. Conclusions

1) Néel theory demonstrates that despite storage near the lunar surface for billions of years, lunar rock magnetism is thermally stable. Uncertainties regarding the origin of the paleofields that existed on the Moon, nonequilibrium iron microstructures, magnetostatic interaction effects, thermal alteration during heating, and the multidomain character of the remanence carriers are likely to be more important than time–temperature effects in the interpretation of lunar paleofields.
2) Single domain grains with blocking temperatures up to ~325–375 °C should have lost some of their remanence due to exposure to temperatures up to 110 °C on the lunar surface. Therefore, remanence carried by such grains is unlikely to be a primary paleomagnetic record. Remanence carried by grains with blocking temperatures below ~125 °C is probably a recent viscous remanence acquired on Earth.
3) Viscous contamination from storage in the Earth field for 10–30 years can be mostly removed by ~1 month of storage at 20 °C in zero field, which should demagnetize single domain grains with blocking temperatures up to 85 °C. Alternatively, the sample can be heated in zero field to 125 °C.
4) The unblocking of magnetism over millions of years implies that crude NRM/SIRM (otherwise known as total REM) measurements may underestimate the lunar paleofield by a factor of two, depending on the blocking temperature and grain size distribution in the rock.
5) Our calculations can be used to assess a variety of other lunar thermal histories including mare volcanism and impact ejecta burial. They can also be used to interpret the magnetism of meteorites, asteroids, and any other iron-bearing bodies in the solar system.
6) Our calculations do not apply to samples dominated by multidomain grains. A complete test of our calculations will require studying predominantly single domain samples with well-documented time-temperature histories.

Acknowledgements

We are most grateful to T. Grove for discussions and E. Mazarico for help with French translations. Reviews and suggestions by Joshua Feinberg and Stuart Gilder helped improve the manuscript. We also thank R. Bennett-Calorio, K. Wills, and M. Pendleton for administrative assistance. This work was supported by the Charles Reed Faculty Initiatives Fund at MIT, the Victor P. Starr Career Development Professorship fund, the NASA Lunar Advanced Science and Exploration Research Program, and the NASA Lunar Science Institute.

References

Anderson, O.L., Isaak, D.G., 2000. Calculated melting curves for phases of iron. Am. Mineral. 85, 376–385.
Arvidson, R., Corzaz, G., Drozd, R.J., Hohenberg, C.M., Morgan, C.J., 1975. Cosmic ray exposure ages of features and events at the Apollo landing sites. Moon 13, 259–276.
Bhadeshia, H.K.D.H., 1985. Diffusional formation of ferrite in iron and its alloys. Prog. Mater. Sci. 29, 321–386.
Bozorth, R.M., 1951. Ferromagnetism. D. Van Nostrand, Princeton. 968 pp.
Cacciamani, G., Keyzer, J.D., Ferro, R., Klotz, U.E., Lacaze, J., Wollants, P., 2006. Critical evaluation of the Fe–Ni, Fe–Ti and Fe–Ni–Ti alloy systems. Intermetallics 14, 1312–1325.
Chong, S.H., Sayles, A., Keyse, R., Atkinson, J.D., Wilson, E.A., 1998. Examination of microstructures and microanalysis of a Fe–9% Ni alloy. Mater. Trans. 39, 179–188.
Chowdhary, S.K., Collinson, D.W., Stephenson, A., Runcorn, S.K., 1987. Further investigations into lunar palaeointensity determinations. Phys. Earth Planet. Inter. 49, 133–141.
Crangle, J., Goodman, G.M., 1971. The magnetization of pure iron and nickel. Proc. R. Soc. Lond. A 321, 477–491.
Cullity, B.D., 1972. Introduction to Magnetic Minerals. Addison-Wesley, Reading, Massachusetts.
Dunlop, D.J., Özdemir, Ö., 1997. Rock Magnetism: Fundamentals and Frontiers. Cambridge University Press, Cambridge, UK. 596 pp.
Dunlop, D.J., Gose, W.A., Pearce, G.W., Strangway, D.W., 1973. Magnetic properties and granulometry of metallic iron in lunar breccia 14313. Proc. Lunar Sci. Conf. 4th, 2977–2990.
Dunlop, D.J., Ozdemir, O., Clark, D.A., Schmidt, P.W., 2000. Time–temperature relations for the remagnetization of pyrrhotite (Fe7S8) and their use in estimating paleotemperatures. Earth Planet. Sci. Lett. 176, 107–116.
Fuller, M., Cisowski, S.M., 1987. Lunar paleomagnetism. In: Jacobs, J.A. (Ed.), Geomagnetism II. Academic Press, New York, pp. 307–455.
Garrick-Bethell, I., Weiss, B.P., Shuster, D.L., Buz, J., 2009. Early lunar magnetism. Science.
Gattacceca, J., Lamali, A., Rochette, P., Boustie, M., Berthe, L., 2007. The effects of explosive-driven shocks on the natural remanent magnetization and the magnetic properties of rocks. Phys. Earth Planet. Inter. 162, 85–98.

Gattaccecaa, J., Bertheb, L., Boustiec, M., Vadeboina, F., Rochettea, P., Resseguierc, T.D., 2008. On the efficiency of shock magnetization processes. Phys. Earth Planet. Inter. 166, 1–10.
Goldstein, J.I., Scout, E.R.D., Chabot, N.L., 2009. Iron meteorites: crystallization, thermal-history, parentbodies, andorigin. Chem. Erde 69, 293–325.
Gose, W.A., Carnes, J.G., 1973. The time dependent magnetization of fine-grained iron in lunar breccias. Earth Planet. Sci. Lett. 20, 100–106.
Gose, W.A., Strangway, D.W., Pearce, G.W, 1973. A determination of the intensity of the ancient lunar magnetic field. Moon 7, 196–201.
Heiken, G.H., Vaniman, D.T., Fench, B.M., 1991. Lunar Sourcebook: A User's Guide to the Moon. Cambridge University Press, Cambridge, UK. 756 pp.
Kuz'min, M.D., 2005. Shape of temperature dependence of spontaneous magnetization of ferromagnets: quantitative analysis. Phys. Rev. Lett. 94, 107204.
Lawrence, K.P., Johnson, C.L., Tauxe, L., Gee, J., 2008. Lunar paleointensity measurements: implications for lunar magnetic evolution. Phys. Earth Planet. Inter. 168 (1-2), 71–87.
Massalski, T.B., 1984. Distinguishing features of massive transformations. Metal. Trans. 15A, 421–425.
Nagata, T., Fisher, R.M., Schwerer, F.C., Fuller, M.D., Dunn, J.R., 1973. Magnetic properties and natural remanent magnetization of Apollo 15 and 16 lunar materials. Proc. Lunar Sci. Conf. 4, 3019–3043.
Nagata, T., Sugiura, N., Fisher, R.M., Schwerer, F.C., Fuller, M.D., Dunn, J.R., 1974. Magnetic properties of Apollo 11–17 lunar materials with special reference to effects of meteorite impact. Proc. Lunar Sci. Conf. 5th, 2827–2839.
Néel, L., 1949. Théorie due trainage magnétique des ferromagnétiques en grains fins avec applications au terres cuites. Ann. Geophys. 5, 99–136.
Nishizawa, T., Ishida, K., 1993. Co–Fe (Cobalt–Iron). In: Okamoto, H. (Ed.), Phase Diagrams of Binary Iron Alloys. ASM International, Materials Park, OH, pp. 93–101.
Pearce, G.W., Gose, W.A., Strangway, D.W., 1973. Magnetic studies on Apollo 15 and 16 lunar samples. Proc. Lunar Sci. Conf. 4, 3045–3076.
Pearce, G.W., Hoye, G.S., Strangway, D.W., 1976. Some complexities in the determination of lunar paleointensities. Proc. Lunar Sci. Conf. 7th, 3271–3297.
Peschard, M., 1925. Contribution to the study of ferro-nickels. Rev. Metall. 22, 430–676.
Pullaiah, G., Irving, E., Buchan, K.L., Dunlop, D.J., 1975. Magnetization changes caused by burial and uplift. Earth Planet. Sci. Lett. 28, 133–143.
Reisener, R.J., Goldstein, J.I., 2003. Ordinary chondrite metallography: Part 1. Fe–Ni taenite cooling experiments. Meteorit. Planet. Sci. 38, 1669–1678.
Reuter, K.B., Williams, D.B., Goldstein, J.I., 1989. Determination of the Fe–Ni phase diagram below 400 °C. Metall. Trans. A 20A, 719–725.
Romig, A.D., Goldstein, J.I., 1980. Determination of the Fe–Ni and Fe–Ni–P phase diagrams at low temperatures (700–300 °C). Metall. Trans. A 11A, 1151–1159.
Ryder, G., Norman, M.D., Score, R.A., 1980. The distinction of pristine from meteorite-contaminated highlands rocks using metal compositions. Proc. Lunar Planet. Sci. Conf. 11th, 471–479.
Sugiura, N., Strangway, D.W., 1980. Comparisons of magnetic paleointensity methods using a lunar sample. Proc. Lunar Sci. Conf. 11th, 1801–1813.
Sugiura, N., Wu, Y.M., Strangway, D.W., Pearce, G.W., Taylor, L.A., 1979. A new magnetic paleointensity value for a 'young lunar glass'. Proc. Lunar Sci. Conf. 10th, 2189–2197.
Swartzendruber, L.J., Itkin, V.P., Alcock, C.B., 1993. Iron–Nickel. In: Okamoto, H. (Ed.), Phase Diagrams of Binary Iron Alloys. ASM International, Materials Park, OH, pp. 256–278.
Tarasov, L.P., 1939. Ferromagnetic anisotropy of low nickel alloys of iron. Phys. Rev. 56, 1245–1246.
Thellier, E., Thellier, O., 1959. Sur l'intensité du champ magnétique terrestre dans le passe historique et geologique. Ann. Geophys. 15, 285–376.
Wasilewski, P., 1974. Magnetic remanence mechanisms in iron and iron–nickel alloys, metallographic recognition criteria and implications for lunar sample research. Moon 9, 335–354.
Wasilewski, P., 1981. Magnetization of small iron–nickel spheres. Phys. Earth Planet. Inter. 26, 149–161.
Weiss, B.P., Kirschvink, J.L., Baudenbacher, F.J., Vali, H., Peters, N.T., MacDonald, F.A., Wikswo, J.P., 2000. A low temperature transfer of ALH84001 from Mars to Earth. Science 290, 791–795.
Wilcox, B.B., Robinson, M.S., Thomas, P.C., Hawke, B.R., 2005. Constraints on the depth and variability of the lunar regolith. Meteorit. Planet. Sci. 40, 695–710.
Wilson, E.A., 1994. The /gamma-> /alpha transformation in low carbon irons. ISIJ Int. 34, 615–630.
Wilson, E.A., Chong, S.H., 2002. Isothermal transformations in an Fe–9% Ni alloy. Metall. Mater. Trans. A 33A, 2425–2431.
Yang, C.-W., Williams, D.B., Goldstein, J.I., 1997. Low-temperature phase decomposition in metal from iron, stony-iron, and stony meteorites. Geochim. Cosmochim. Acta 61, 2943–2956.